

Magnetic interlayer coupling between ferromagnetic SrRuO_3 layers through a SrIrO_3 spacer

Cite as: J. Appl. Phys. **131**, 133902 (2022); <https://doi.org/10.1063/5.0087098>

Submitted: 01 February 2022 • Accepted: 18 March 2022 • Published Online: 06 April 2022

 Lena Wysocki,  Sven Erik Ilse,  Lin Yang, et al.





View Online



Export Citation



CrossMark




Instruments for Advanced Science

- Knowledge,
- Experience,
- Expertise


[Click to view our product catalogue](#)

Contact Hiden Analytical for further details:
www.HidenAnalytical.com
info@hideninc.com




Gas Analysis

- dynamic measurement of reaction gas streams
- catalysis and thermal analysis
- molecular beam studies
- dissolved species probes
- fermentation, environmental and ecological studies




Surface Science

- UHVTPD
- SIMS
- end point detection in ion beam etch
- elemental imaging - surface mapping



Plasma Diagnostics

- plasma source characterization
- etch and deposition process reaction kinetic studies
- analysis of neutral and radical species



Vacuum Analysis

- partial pressure measurement and control of process gases
- reactive sputter process control
- vacuum diagnostics
- vacuum coating process monitoring

Magnetic interlayer coupling between ferromagnetic SrRuO₃ layers through a SrIrO₃ spacer

Cite as: J. Appl. Phys. **131**, 133902 (2022); doi: [10.1063/5.0087098](https://doi.org/10.1063/5.0087098)

Submitted: 1 February 2022 · Accepted: 18 March 2022 ·

Published Online: 6 April 2022



Lena Wysocki,^{1,a)} Sven Erik Ilse,^{2,a)} Lin Yang,¹ Eberhard Goering,² Felix Gunkel,³ Regina Dittmann,³ Paul H. M. van Loosdrecht,¹ and Ionela Lindfors-Vrejoiu^{1,a)}

AFFILIATIONS

¹Institute of Physics II, University of Cologne, Cologne, Germany

²Max Planck Institute for Intelligent Systems, Stuttgart, Germany

³Peter Grünberg Institut (PGI-7), Forschungszentrum Jülich GmbH, Jülich, Germany

^{a)}Authors to whom correspondence should be addressed: wyssocki@ph2.uni-koeln.de; ilse@is.mpg.de; and vrejoiu@ph2.uni-koeln.de

ABSTRACT

A key element to tailor the properties of magnetic multilayers is the coupling between the individual magnetic layers. In the case of skyrmion hosting multilayers, coupling of skyrmions across the magnetic layers is highly desirable. Here, the magnetic interlayer coupling was studied in epitaxial all-oxide heterostructures of ferromagnetic perovskite SrRuO₃ layers separated by spacers of the strong spin-orbit coupling oxide SrIrO₃. This combination of oxide layers is being discussed as a potential candidate system to host Néel skyrmions. First order reversal curve (FORC) measurements were performed in order to distinguish between magnetic switching processes of the individual layers and to disentangle the signal of soft magnetic impurities from the sample signal. Additionally, FORC investigations enabled us to determine whether the coupling between the magnetic layers is ferromagnetic or antiferromagnetic. The observed interlayer coupling strength was very weak for the heterostructure with a two monolayer (ML) thick SrIrO₃ spacer, and no coupling was observed for spacers of 6 and 12 ML thickness. The decoupling of the magnetic SrRuO₃ layers due to the SrIrO₃ spacer is a disadvantage for the study of skyrmions in such multilayers and indicates that other oxides have to be identified for realizing strong magnetic coupling.

Published under an exclusive license by AIP Publishing. <https://doi.org/10.1063/5.0087098>

I. INTRODUCTION

Heterostructures with ultrathin layers of the ferromagnetic perovskite oxide SrRuO₃ have been in focus recently due to the proposal of hosting tiny Néel-type skyrmions.^{1–3} In a multilayer, if skyrmions are formed, their ferromagnetic coupling across the stack has to be achieved, as in metallic multilayers.^{4–6} Although several studies addressed the formation of skyrmions by observing unconventional features in the Hall effect resistance loops of SrRuO₃/SrIrO₃ and other heterostructures involving ultrathin SrRuO₃ layers, the existence of topologically non-trivial textures in SrRuO₃ thin films is still under debate,^{1–3,7–15} and the interlayer coupling in SrRuO₃-based multilayers has received little investigation.¹⁶ Experimental studies of the magnetic interlayer coupling

between SrRuO₃ layers were performed only in multilayers with spacers that are not expected to induce interfacial Dzyaloshinskii–Moriya interaction (DMI), such as LaNiO₃ or SrTiO₃.^{17,18} Yang *et al.* achieved strong ferromagnetic coupling of the SrRuO₃ layers by introducing a four monolayer (ML) thick metallic LaNiO₃ spacer, while weak ferromagnetic coupling was observed for the separation of the SrRuO₃ layers by 2 ML of LaNiO₃ (1 ML is about 0.4 nm thick for all the perovskites under discussion here and represents the dimensions of a pseudocubic cell).¹⁷ Insulating SrTiO₃ spacers, 1.6–2.5 nm thick, were found to result at best in weak magnetic coupling of two epitaxial SrRuO₃ layers in the study by Herranz *et al.*¹⁸ In our previous work,¹⁹ the interlayer coupling between SrRuO₃ layers separated by an asymmetric spacer of the

strong spin-orbit coupling oxide SrIrO_3 and the large bandgap insulator SrZrO_3 was addressed. Weak ferromagnetic coupling was observed with enhanced coupling strength for the reduction of the total spacer thickness from 1.6 to 0.8 nm.¹⁹ However, for $\text{SrRuO}_3/\text{SrIrO}_3$ multilayers with 2 ML thick SrIrO_3 (about 0.8 nm), where the SrIrO_3 was discussed to induce interfacial DMI,^{1,2,16,20} there are only theoretical calculations and no experimental data, which predict that ferromagnetic coupling between the SrRuO_3 layers is more favorable than an antiferromagnetic type of coupling.¹⁶

Here, we address experimentally the magnetic interlayer coupling in SrRuO_3 - SrIrO_3 multilayers with various spacer thickness by means of superconducting quantum interference device (SQUID) magnetometry (full and minor hysteresis loops) and first order reversal curve measurements (FORC). The FORC method has proven to provide valuable information in many different systems that are inaccessible for conventional magnetometry measurements. For example, microstructural information without actual lateral resolution in microstructured and model magnetic systems,^{21–24} information about a coercive and interaction field distribution in permanent hard magnetic systems,^{25–27} as well as interaction strength and interaction type between different magnetic components in systems^{21,27} can be achieved. Performing minor hysteresis loops and FORC measurements enabled us to quantify the sign and strength of the magnetic interlayer coupling between the SrRuO_3 layers for various SrIrO_3 spacer thicknesses. For the heterostructure with only a 2 ML SrIrO_3 spacer, which is the spacer thickness that was often used in previous magnetotransport studies of SrRuO_3 - SrIrO_3 multilayers,^{1,2,14,20} the minor loops showed a small positive shift with respect to the major hysteresis loops at temperatures of minimum 40 K, indicating that the coupling turned weakly antiferromagnetic. However, the estimated coupling strength of about $-7 \mu\text{J}/\text{m}^2$ at 40 K is too weak to serve our aim of obtaining strong magnetic coupling between SrRuO_3 layers. To test the possibility of achieving strong magnetic interlayer coupling between the SrRuO_3 layers, the SrIrO_3 spacer thickness was increased to 6 and 12 ML. In addition to the commonly observed thickness dependence of the interlayer coupling strength mediated by exchange or magnetostatic interactions, SrIrO_3 offers the possibility to address the influence of the electronic properties of the spacer on the interlayer coupling. SrIrO_3 is a paramagnetic semi-metal with a Fermi surface that consists of electron- and holelike pockets²⁸ in its bulk form and thick films; however, the transition to an insulating state can be induced in SrIrO_3 thin films by the reduction of the film thickness in the ultrathin limit^{28–30} and by tailoring of the epitaxial strain.^{31,32} A resistivity increase was observed upon temperature enhancement in these SrIrO_3 layers of minimum 4 ML thickness that indicated the metallic properties.³⁰ In contrast, a 20 nm thick SrIrO_3 film showed only weakly temperature-dependent resistivity in the study by Gruenewald *et al.*³³ In our current study, it was, therefore, expected that the 2 ML SrIrO_3 spacer is insulating and might undergo a transition from the insulating to the (semi-)metallic state, upon a thickness increase. In the case of a transition to the semimetallic state with clear temperature-dependent resistivity, the influence of the SrIrO_3 electronic transport properties on the interlayer coupling could be addressed in our study. It turned out that the coupling strength did not increase upon the increase of the spacer thickness to 12 MLs

and the two SrRuO_3 layers stayed decoupled. Resistivity investigations of SrIrO_3 reference films show that they are semimetallic with very weakly temperature-dependent behavior. Thus, SrIrO_3 layers may be unsuitable as spacers for achieving strong magnetic coupling between ferromagnetic SrRuO_3 , and other oxide layers ought to be considered for realizing this end.

II. SAMPLE DESIGN AND EXPERIMENTAL METHODS

For investigating the type and strength of the magnetic coupling of the ferromagnetic SrRuO_3 layers, a set of heterostructures with two ferromagnetic SrRuO_3 layers of distinct thicknesses was designed. To make use of the thickness dependence of the coercive field H_c and ferromagnetic transition temperature T_c of SrRuO_3 thin films,³⁴ each multilayer was composed of two separated SrRuO_3 layers with 6 ML and 18 ML thicknesses. The 18 ML thick SrRuO_3 was deposited directly on the SrTiO_3 (100) substrate, while the top 6 ML SrRuO_3 layer was grown on top of the spacer layer, as illustrated in the scheme of the heterostructure design in Fig. 1. For heterostructure RIR2, with the thinnest (2 MLs) SrIrO_3 spacer of this study, the 6 ML SrRuO_3 layer was additionally capped by 2 ML SrIrO_3 . This capping layer was added so that we had for the 6 ML SrRuO_3 the same boundary conditions on both interfaces, as this kind of unit was employed by us in the study of symmetric $\text{SrRuO}_3/\text{SrIrO}_3$ multilayers in a recent work.¹⁴ We think that the capping layer of the RIR2 heterostructure plays no active role in the magnetic interlayer coupling studied here, for which only the spacer layer between the two magnetic layers has high relevance.

The heterostructures were fabricated by pulsed-laser deposition (PLD), using a KrF excimer laser with 248 nm wavelength. The multilayers were grown on SrTiO_3 (100) substrates. The substrates were etched in an NH_4F -buffered HF solution and annealed in air at 1000 °C for 2 h to achieve uniform TiO_2 termination of the surface. During the growth, the deposition temperature was 650 °C, the oxygen pressure was kept at 0.133 mbar, and the laser fluence was set to about $2 \text{ J}/\text{cm}^2$. We used a 5 Hz repetition rate for the SrRuO_3 and 1 Hz for SrIrO_3 . In order to ensure a smooth epitaxial growth for enhanced thicknesses of the SrIrO_3 spacer, the deposition temperature was increased for the heterostructure RIR12 to 700 °C. Employing *in situ* high-energy electron diffraction (RHEED) enabled the precise control of the SrIrO_3 layer thickness, which grew in a layer-by-layer mode [see Fig. S1(b) in the [supplementary material](#)]. Atomic force microscopy (AFM) investigations confirmed the smooth topography of the heterostructure surface resembling the stepped terrace structure of the SrTiO_3 (100) substrates, which indicates the pseudomorphic, crystalline growth. Further details on the thin film deposition and structural characterization can be found in the [supplementary material](#).

The magnetic interlayer coupling was investigated by a combination of conventional SQUID magnetometry (temperature-dependent and magnetic field-dependent magnetic moment measurements) and FORC investigations. The study was complemented by a polar magneto-optical Kerr effect (p-MOKE) and Hall voltage measurements for selected samples. All Hall measurements were performed in the van der Pauw geometry in a custom-built setup.

SQUID magnetometry was performed by a commercially available SQUID magnetometer (MPMS-XL, Quantum Design, Inc.).

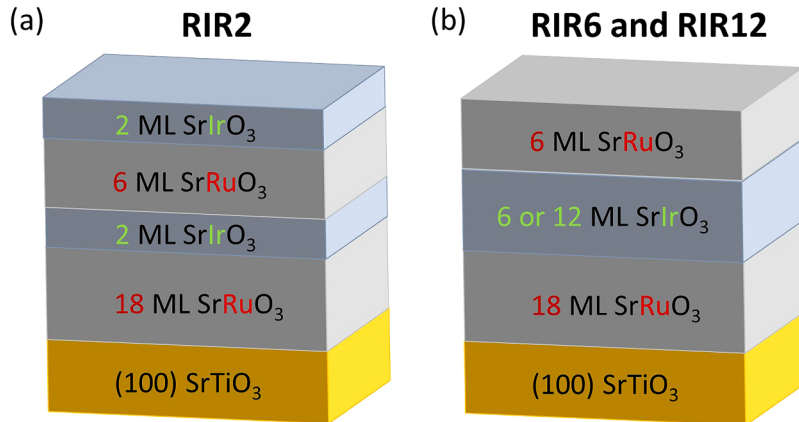


FIG. 1. Schematics of the design of heterostructure RIR2 with a 2 ML SrIrO₃ spacer and a capping layer (a). In (b) is the scheme of the heterostructures RIR6 and RIR12, with a 6 or 12 ML SrIrO₃ spacer, respectively, and no capping layer.

In order to extract the magnetic response of the ferromagnetic SrRuO₃ layers, the linear contribution of the diamagnetic SrTiO₃ substrate was subtracted by linear fitting in the high magnetic field range. Furthermore, the nonlinear magnetic moment measured above the Curie temperature of the SrRuO₃ layers was subtracted to correct the additional background response originating from magnetic impurities introduced most likely during the required sample cutting (see Sec. II of the [supplementary material](#)).

The FORC measurements were performed with a SQUID magnetometer (MPMS 3, Quantum Design, Inc.). Processing of raw data was done with LeXtender,³⁵ and the FORC densities were calculated using the gFORC algorithm.³⁶ For the FORC study, a set of minor loops with various reversal fields was performed. Before each minor loop, the sample was saturated in a positive magnetic field of 5 T. Then, the external magnetic field was decreased to the required reversal field H_r . The first order reversal curve was determined by measuring the magnetic moment when the magnetic field was increased from H_r to saturation in positive magnetic fields.^{21,26,36} This procedure was repeated with step-like decreasing of the reversal field until the reversal field reached negative saturation. The FORC density was calculated by the mixed second derivative of the magnetic moment surface,

$$\rho(H, H_r) = -\frac{1}{2} \frac{\partial^2 m(H, H_r)}{\partial H \partial H_r}. \quad (1)$$

The FORC density was then transformed on the axes of the coercive field H_c and the interaction field H_u via

$$H_u = \frac{1}{2}(H + H_r), \quad H_c = \frac{1}{2}(H - H_r). \quad (2)$$

From the FORC density, plotted as a function of the interaction field and the coercive field, the sign of the magnetic interlayer coupling can be assessed.

III. RESULTS

A. Magnetic interlayer coupling for heterostructures with a 2 ML thick SrIrO₃ spacer

Summarized in [Figs. 2\(a\) and 2\(b\)](#) are major and minor magnetic hysteresis loops for the heterostructure RIR2 (2 MLs SrIrO₃/6 MLs SrRuO₃/2 MLs SrIrO₃/18 MLs SrRuO₃ on SrTiO₃) at representative temperatures of 10 and 80 K. The magnetic field was applied perpendicular to the thin film surface for the presented measurements. The hysteresis loops, acquired by SQUID magnetometry, were corrected by the subtraction of the diamagnetic background of the SrTiO₃ substrate and magnetic impurities, following the procedure described in Sec. II of the [supplementary material](#).

The magnetization of the heterostructure RIR2 reverses its orientation in a two-step reversal process, indicating at best weak coupling of the two SrRuO₃ layers. Since the 18 ML thick SrRuO₃ layer has a larger magnetic moment than the thinner SrRuO₃ layer, it can be concluded that the thicker layer is the magnetically softer layer at 10 K. At elevated temperatures, such as 80 K, the thinner 6 ML SrRuO₃ layer is magnetically softer and switches at smaller magnetic fields than the 18 ML SrRuO₃ layer, as it has been shown already in our previous study on similar SrRuO₃-based heterostructures.¹⁹ The temperature dependence of the switching fields of the two ferromagnetic layers of this particular heterostructure RIR2 is shown in [Fig. S4\(b\)](#) of the [supplementary material](#).

In addition to the sharp two-step magnetization reversal, the magnetic hysteresis loops possess a tail in the high magnetic field range, which can be related most likely to strongly pinned domains in the bottom SrRuO₃ layers deposited directly on the SrTiO₃ (100) substrate.³⁷

The minor loop of heterostructure RIR2, drawn in blue in [Fig. 2\(a\)](#), did not show a measurable shift with respect to the major hysteresis loop at 10 K, showing that the two SrRuO₃ layers of the heterostructure are indeed magnetically decoupled. In contrast, the minor loop of the heterostructure RIR2 is shifted by +30 mT to higher magnetic fields at 80 K, as indicated by the red lines in the inset of [Fig. 2\(b\)](#). Such a positive shift of the minor loop with

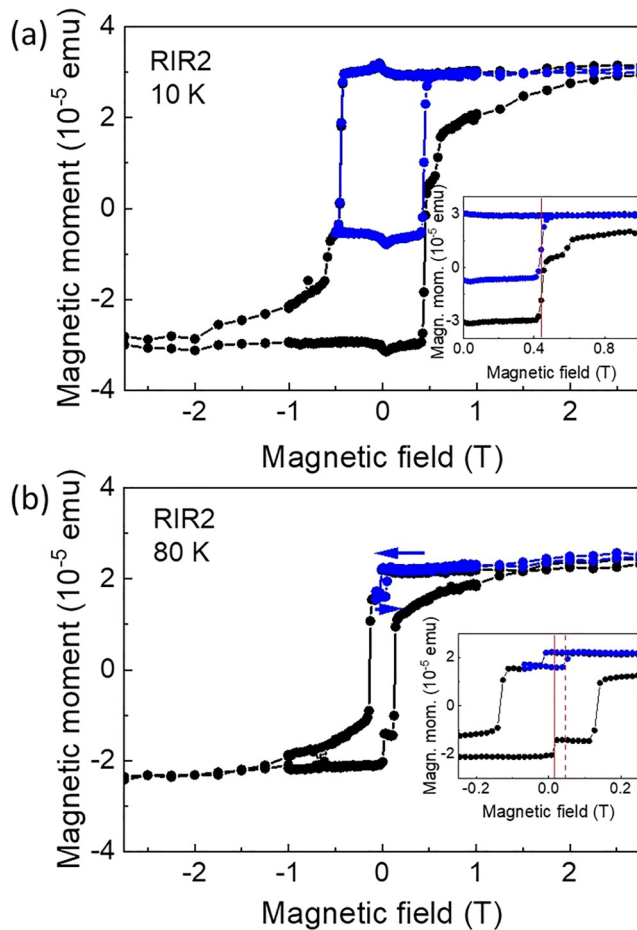


FIG. 2. (a) Major (black) and minor (blue) magnetic hysteresis loops for the heterostructure RIR2 with a 2 ML SrIrO_3 spacer at 10 (a) and 80 K (b). The magnetic field was applied perpendicular to the thin film surface. The minor loops were carried out between 5 and -0.5 T (a) and -0.07 T (b). The minor loop at 10 K (a) does not show a measurable shift. At 80 K (b), the switching field (during the backward sweep) of the minor loop (red dashed line) is shifted by $+30$ mT with respect to the reversal field of the magnetically softer layer during the major loop (solid red line).

respect to the full loop can be an indication for antiferromagnetic coupling of the two SrRuO_3 layers (see, for instance, Refs. 38–40). According to van der Heijden *et al.*, the magnetic coupling strength is directly proportional to the difference of the switching fields of the magnetically softer layer of the major loop and of the minor loop.³⁸ As described in detail in Sec. IV of the [supplementary material](#), we estimated a coupling strength of $-5 \mu\text{J}/\text{m}^2$ at 80 K, increasing to $-7 \mu\text{J}/\text{m}^2$ at 40 K. This coupling strength is very weak: In our previous study on asymmetric $\text{SrIrO}_3/\text{SrZrO}_3$ spacers, we observed weak ferromagnetic coupling on the order of $35 \mu\text{J}/\text{m}^2$ for a 1 ML SrIrO_3 /1 ML SrZrO_3 spacer (about 0.8 nm total spacer thickness). For 2 ML thick LaNiO_3 spacers between SrRuO_3 layers, a coupling strength of $106 \mu\text{J}/\text{m}^2$ at 10 K was

reported.¹⁷ As shown in Fig. S4 of the [supplementary material](#), for heterostructure RIR2, the minor loop shift is almost temperature independent between 40 and 100 K when the 6 ML top SrRuO_3 layer is the magnetically softer layer of the heterostructure. Thus, the coupling strength, which is directly proportional to the magnetization of the magnetically softer layer,³⁸ decreases for increasing temperature above 40 K, following the temperature dependence of the magnetization of the thinner SrRuO_3 layer.

To confirm the sign and order of magnitude of the minor loop shifts, determined from the magnetometry measurements, Kerr rotation measurements were performed at 10 and 80 K (see Fig. S3 in the [supplementary material](#)). The Kerr rotation angle, determined in the polar MOKE geometry, scales linearly with the perpendicular component of the magnetization but is not influenced by magnetic impurities at the backside or on the edges of the sample for our measurements in reflection geometry and, therefore, a useful probe of the qualitative interlayer coupling. In agreement with our results from the SQUID investigations, the minor loop at 10 K [Fig. S3(a) in the [supplementary material](#)] is not shifted within the magnetic field accuracy, while the minor loop at 80 K is also shifted by $+38$ mT [Fig. S3(b) in the [supplementary material](#)].

The magnetic interlayer coupling in the heterostructure RIR2 was further addressed by FORC measurements. We show here the FORC loops performed at 10 K (Fig. 3) and 80 K (Fig. 4).

In Fig. 3(a), the set of minor loops of heterostructure RIR2 at 10 K is shown. All minor loops were corrected by the subtraction of the diamagnetic contribution originating from the SrTiO_3 substrate. The soft magnetic contribution visible in the minor loops at small magnetic fields is related to magnetic impurities, often introduced during the sample cutting process, as mentioned earlier. Additionally, the two-step reversal of the magnetization was observed for the minor loops that started close to negative saturation. From these minor loops, the FORC density was calculated according to Eq. (1) and is shown in Fig. 3(b). Three general features are present in the FORC density at 10 K. The positive peaks (I) and (II) correspond to the reversal of the two ferromagnetic SrRuO_3 layers. The intensity of the peaks is proportional to magnetization of the respective layer. Hence, the more intense peak (II) is related to the switching of the 18 ML bottom SrRuO_3 layer and (I) to the 6 ML thin SrRuO_3 layer. The positions of the center of the peaks at 620 mT (I) and 450 mT (II) are in good agreement with the switching fields determined from the major magnetization hysteresis loops [see Fig. S4(b) in the [supplementary material](#)]. The FORC investigations of heterostructure RIR2 did not show any hints of the coupling of the two ferromagnetic SrRuO_3 layers at 10 K. The additional feature located at tiny magnetic field values is the reversible ridge, which is dominated by magnetically soft, reversible contributions originating mainly from magnetic impurities. In the case of the SQUID hysteresis loop (Fig. 2), these contributions were removed by subtraction of the hysteresis loop measured above the transition temperature of the SrRuO_3 layers and, therefore, related to high T_c magnetic impurities (see Sec. II of the [supplementary material](#) for further details). To confirm that the reversible ridge is dominated by the contribution of these magnetic impurities, the FORC density presented in Fig. 3(b) was reintegrated with the exclusion of the contribution between -0.05 T

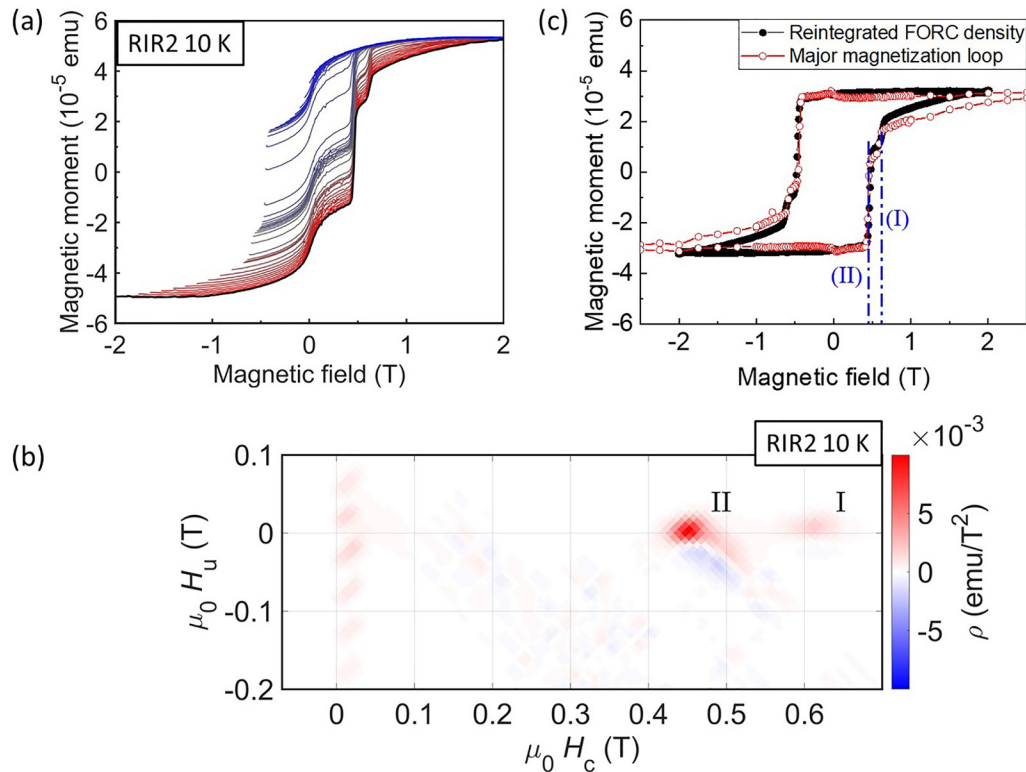


FIG. 3. First order reversal curve study of the heterostructure RIR2 at 10 K. The magnetic field was applied perpendicular to the heterostructure surface. The measured minor loops, corrected for the diamagnetic contribution originating from the substrate, are presented in (a). The color of the respective minor loops changes from red to blue for increasing reversal fields. The FORC density ρ plotted as a function of the coercive field H_c and the interaction field H_u at the corresponding temperatures is shown in (b). Positive FORC density peaks are drawn in red and negative ones in blue. Features (I) and (II) correspond to the magnetization switching of the 6 ML (I) and 18 ML SrRuO_3 (II) layer, respectively. Shown in (c) is the comparison of the major magnetization loop (red), corrected by the subtraction of the diamagnetic substrate and the magnetic impurity contribution (see the [supplementary material](#)), and the reintegrated FORC density (black) after removal of the soft magnetic contribution of the reversible ridge between $-0.05\text{ T} < \mu_0 H_c < 0.1\text{ T}$ and $-1.5\text{ T} < \mu_0 H_u < 1.5\text{ T}$. The dashed blue lines in (c) indicate the magnetic fields of the center positions of peaks (I) and (II) of the FORC density.

$< \mu_0 H_c < 0.1\text{ T}$ and $-1.5\text{ T} < \mu_0 H_u < 1.5\text{ T}$. Such integration of the FORC density was possible because features (I) and (II) originating from the magnetization reversal of the layers were sufficiently separated from the reversible ridge. The integration yielded half of the hysteresis loop from -2 to 2 T and was mirrored at both x and y axes in order to reconstruct the full hysteresis loop. Plotted in Fig. 3(c) is the comparison of the reconstructed hysteresis loop of the FORC study (black) and the conventional major magnetization loop (red), which has been corrected for the magnetic impurity contribution. Both hysteresis loops are in good agreement, and the switching fields of the two SrRuO_3 layers are identical for both techniques within a few mT. The agreement of both hysteresis loops supports our expectation that the reversible ridge is dominated by uncorrelated magnetic impurities that do not influence the switching fields of the magnetic SrRuO_3 layers of the heterostructure. This shows that the reintegration of the FORC density without the reversal ridge can be used in this case to obtain a hysteresis loop where the contribution of the soft magnetic impurity is

removed without the need for an additional measurement above the transition temperature of SrRuO_3 .

The FORC study of heterostructure RIR2 at 80 K is summarized in Fig. 4. Also, the minor loops measured at 80 K, displayed in Fig. 4(a), show a two-step magnetization reversal. At 80 K, the 6 ML thin SrRuO_3 switches at smaller magnetic fields than the 18 ML thick bottom SrRuO_3 layer. In the FORC density, shown in (b), feature (I) corresponds again to the reversal of 6 MLs SrRuO_3 , while feature (II) originates from the magnetization switching of the 18 ML thick SrRuO_3 layer. In contrast to the FORC density map at 10 K, an additional positive-negative peak pair (structure III) is present at a finite interaction field [see Fig. 4(b)] at 80 K. According to previous FORC studies on well defined systems of coupled microarrays and on NdFeB samples with components with different coercivities, such additional positive-negative peak pairs are characteristic for magnetic coupling between two different magnetic sites and denominated as the so-called interaction peak.^{21,26} The relative position of the positive and negative part of the

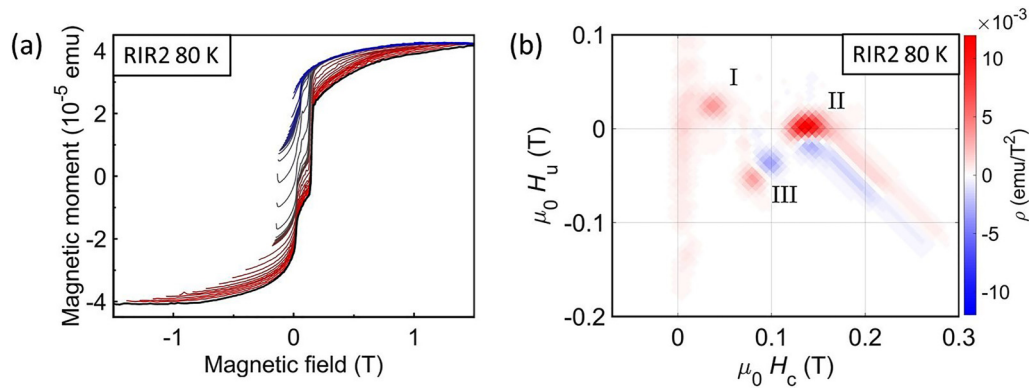


FIG. 4. FORC study of the heterostructure RIR2 at 80 K with the magnetic field applied perpendicular to the heterostructure surface. The measured minor loops, corrected for the diamagnetic contribution originating from the substrate, are shown in (a). The color of the respective minor loops changes from red to blue for increasing reversal fields. The FORC density ρ is plotted in (b) as a function of the coercive field H_c and the interaction field H_u . Positive FORC density peaks are shown in red and negative ones in blue. Features (I) and (II) correspond to the magnetization switching of the 6 ML (I) and 18 ML SrRuO₃ (II) layer, respectively. The additional peak pair (III) at 80 K is the interaction peak indicating antiferromagnetic coupling. The additional feature located along $H_c = 0$ T is the reversible ridge.

interaction peak with respect to each other yields information about the nature of the coupling. As shown in Ref. 21, the coupling is antiparallel if the negative FORC density part of the interaction peak is at higher coercive and interaction fields than the positive part of the interaction peak and parallel if it is vice versa. According to this, the interaction peak in Fig. 4(b) shows that the SrRuO₃ layers in sample RIR2 are coupled antiparallel at 80 K, which confirms our observation from the conventional SQUID magnetometry. If an exchange bias between a ferromagnet and an antiferromagnet was present, this would lead most likely to a positive peak in the FORC density, which is elongated along the interaction field⁴¹ rather than a positive–negative peak pair.

The FORC density of a SrRuO₃-based heterostructure in which the ferromagnetic layers are coupled weakly ferromagnetically is presented in the [supplementary material](#) for comparison. In this heterostructure RIZR1, the two SrRuO₃ layers were weakly ferromagnetically coupled through a spacer of 1 ML SrIrO₃ and 1 ML SrZrO₃. The FORC density, plotted in Fig. S5 of the [supplementary material](#), also shows two positive peaks related to the magnetization reversal of the magnetization of the two SrRuO₃ layers. The observed interaction peak shows the positive FORC density at higher coercive and interaction fields than the negative peak, which indicates the ferromagnetic coupling between the SrRuO₃ layers.²¹

The weak antiferromagnetic coupling between SrRuO₃ in heterostructure RIR2, which was observed only above 40 K, cannot originate from direct coupling via pinholes, which would lead to trivial ferromagnetic coupling.^{42,43} On the other hand, we emphasize at this point that the coupling of the two SrRuO₃ layers separated by 2 MLs SrIrO₃ was found to be very sensitive to the existence of (pin-)holes in the heterostructure. As presented in Fig. S8 of the [supplementary material](#), a second heterostructure where holes of nanometer depth were observed by atomic force microscopy showed weak ferromagnetic coupling. In contrast, atomic force microscopy did not show the existence of holes in any of the heterostructures RIR2, RIR6, and RIR12 so that it can

be concluded that the density of pinholes connecting the two SrRuO₃ layers is most likely small for these samples. The weak antiferromagnetic coupling was observed only in heterostructure RIR2 with a 2 ML SrIrO₃ spacer and with a small density of holes seen by AFM.

Antiferromagnetic coupling could be induced by magneto-static Néel's coupling due to correlated surface roughness^{44,45} in the case of strong perpendicular magnetic anisotropy or magnetic exchange coupling by tunneling of spin-polarized electrons through the insulating barrier.^{39,46,47} However, due to the decrease of the absolute value of the coupling strength J_C [calculated with Eq. (1) in the [supplementary material](#)] with increasing temperature, the weak coupling can most likely not be explained within the model of quantum interference effects, which predicts an increase for increasing temperatures in the case of insulating spacers⁴⁷ (for further details on the validity of the approximations made within this model, see Sec. IV of the [supplementary material](#)). Moreover, the orange-peel coupling fields,⁴⁸ expected for the roughness induced by the miscut substrate, would be too small to explain the observed weak antiferromagnetic coupling.

One possible coupling mechanism, which is qualitatively consistent with the observed temperature dependence of the weak antiferromagnetic interlayer coupling in heterostructure RIR2, might be the model of domain replication in the hard layer via magnetostatic interactions, as proposed by Nistor.⁴⁹ When the magnetic field required to reverse the magnetization of the soft layer during the minor loops is close to the nucleation field of the hard layer, inversed domains in the soft layer will generate stray fields that can induce so-called replicated domains in the hard layer acting as a negative bias field during the second half of the minor loop.^{49,50}

Although the antiferromagnetic coupling in heterostructure RIR2 was detectable by FORC and SQUID minor loop investigations above 40 K, its maximum strength of $-7 \mu\text{J}/\text{m}^2$ is very weak¹⁹ so that the layers switch their magnetizations almost independently. We stress here that the observation of this tiny coupling

is not the key message of this work, as our aim is to figure out if strong ferromagnetic coupling is possible when SrIrO_3 is used as a spacer layer.

B. Magnetic interlayer coupling for heterostructures with thicker (6 ML and 12 ML) SrIrO_3 spacers

In order to explore if strong ferromagnetic coupling is possible when SrIrO_3 is used as a spacer, we increased its thickness. We studied heterostructures with spacers that are 6 ML and 12 ML thick. If this thickness increase led to a significant change of the SrIrO_3 electronic transport properties, a major impact on the interlayer exchange coupling might be expected, as it was achieved in SrRuO_3 -based heterostructures separated by LaNiO_3 spacers.¹⁷ The full and minor magnetic hysteresis loops of heterostructure RIR6 (a 6 ML SrIrO_3 spacer) at 50 and 80 K, acquired by SQUID magnetometry, are shown in Figs. 5(a) and 5(b). The major hysteresis loops of the heterostructure RIR6 indicate a two-step reversal of the magnetization, similar to heterostructure RIR2. At 50 K, the switching at 0.1 T originates from the magnetization reversal of the 6 ML SrRuO_3 layer, while the step at 0.25 T is related to the switching of the 18 ML SrRuO_3 layer, which is the magnetically harder layer at

50 K. Such a two-step switching process indicates again the decoupling or weak magnetic interlayer coupling. To determine the interlayer coupling strength, the reversal fields of the minor loop were compared to the switching behavior of the magnetically softer layer during the full loop. As highlighted in the inset of Fig. 5(a), the minor loop switching field is equal to the switching field of the major loop. This shows a minor loop shift and, therefore, the coupling strength is zero (see Sec. IV in the [supplementary material](#) for further details on the calculation). The two SrRuO_3 layers are fully decoupled by 6 ML SrIrO_3 at 50 K. Also, at 80 K, where weak antiferromagnetic coupling was observed for heterostructure RIR2, the minor loop is not shifted in the case of heterostructure RIR6 [see the inset of Fig. 5(b)]. As shown in Fig. 5(c), such equality of the switching fields of a minor loop (drawn as blue triangles) and a major loop (full symbols) was observed at all temperatures investigated for heterostructure RIR6. The absence of a measurable minor loop shift shows that a 6 ML SrIrO_3 spacer decouples the two ferromagnetic SrRuO_3 layers fully at all temperatures.

Increasing the thickness of the SrIrO_3 spacer to 12 MLs was still insufficient to result in measurable magnetic coupling of the two SrRuO_3 layers of heterostructure RIR12. As shown by the hysteresis loop measurements at 50 K in Fig. 5(d), the magnetic

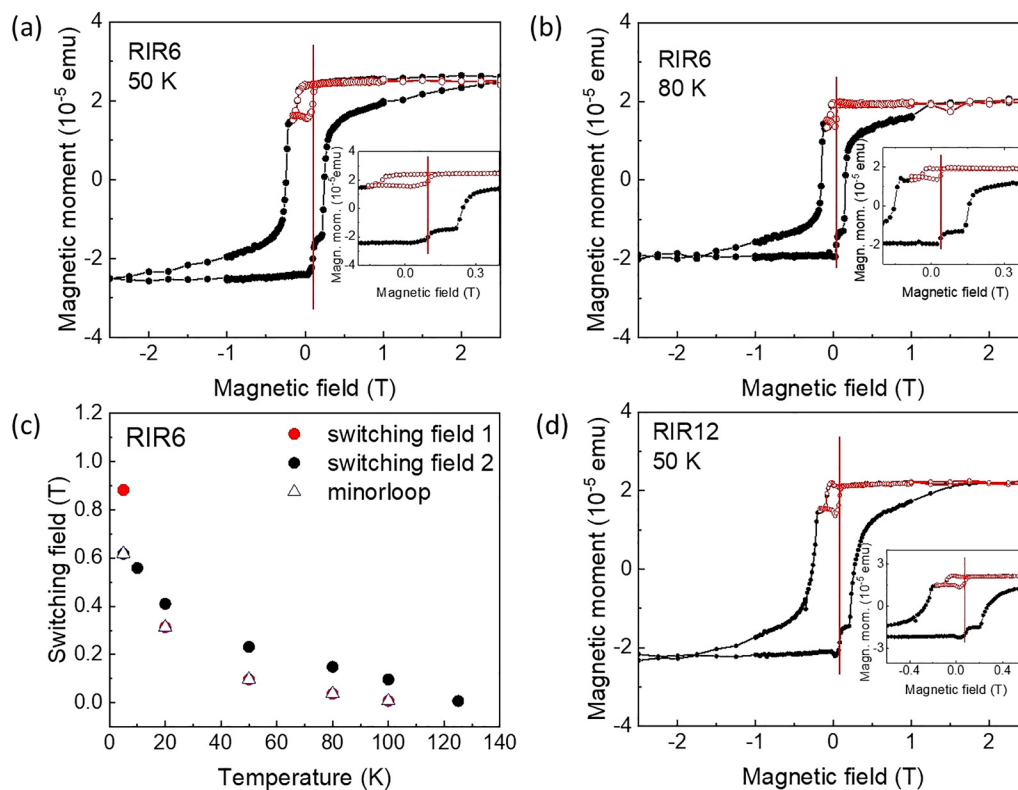


FIG. 5. Full and minor hysteresis loops of the magnetic moment of heterostructure RIR6 with a 6 ML SrIrO_3 spacer at 50 K (a) and 80 K (b). (c) Temperature dependence of the switching fields of the two SrRuO_3 layers with 18 ML (switching field 2) and 6 ML (switching field 1) thicknesses and the switching fields determined from minor loop experiments for the heterostructure RIR6. (d) Major and minor hysteresis loops of the magnetic moment of heterostructure RIR12 with a 12 ML SrIrO_3 spacer at 50 K. The magnetic field was applied perpendicular to the surfaces of the heterostructures.

hysteresis is consistent with a two-step reversal of the magnetization. The minor loop is not shifted within the magnetic field accuracy, indicating the decoupling of the two ferromagnetic layers. The decoupling of the SrRuO₃ layers was confirmed by a magnetotransport study of heterostructure RIR12, presented in Sec. VI of the [supplementary material](#).

The decoupling of the ferromagnetic SrRuO₃ layers, observed in a broad temperature range and consistently for the heterostructures RIR6 and RIR12 with spacer thicknesses above the limit for which a (semi-) metal-to-insulator transition was reported, indicates that an SrIrO₃ spacer may not be a suitable choice for enabling exchange mediated coupling in these heterostructures. In contrast to LaNiO₃ spacer layers,¹⁷ the semimetallic SrIrO₃ layers may not permit the strong ferromagnetic coupling of SrRuO₃ layers, which would be relevant in the context of skyrmion formation in SrRuO₃-SrIrO₃ multilayers.^{14,16} The SrIrO₃ resistivity was investigated by reference sample measurements (bare films grown on SrTiO₃), shown in detail in the [supplementary material](#), because the SrIrO₃ spacer resistivity could not be measured directly for our heterostructures when the SrIrO₃ was sandwiched between the metallic SrRuO₃ layers. The resistivities of these 6 ML and 12 ML SrIrO₃ reference thin films showed very weak temperature dependence with a small resistivity increase for decreasing temperature, as it was also observed in 20 nm SrIrO₃ deposited on SrTiO₃³³ or when sandwiched between LaMnO₃.⁵¹ In the latter case, Skoropata *et al.* considered multilayers of LaMnO₃/SrIrO₃ particularly for the purpose of obtaining skyrmions; however, the magnetic interlayer coupling was overlooked in this study, despite its importance for the observation of skyrmions by imaging techniques.⁵¹

Based on the observed semimetallic behavior of the 6 ML and 12 ML SrIrO₃ reference samples discussed in the [supplementary material](#), also, the SrIrO₃ spacers of the heterostructures are likely semimetallic with similar resistivity behavior, and this enables strong ferromagnetic coupling of the SrRuO₃ layers.

IV. CONCLUSION

The magnetic interlayer coupling between ferromagnetic SrRuO₃ epitaxial layers separated by the strong spin-orbit coupling SrIrO₃ was investigated by the combination of conventional SQUID magnetometry and FORC measurements. The minor loops of the heterostructure with 2 MLs of an SrIrO₃ spacer showed a small shift to a higher magnetic field above 40 K, indicating very weak antiferromagnetic coupling of about $-7 \mu\text{J}/\text{m}^2$. The minor loop of a second heterostructure with a 2 ML SrIrO₃ spacer, which exhibited nanometer-deep holes in the surface topography, showed only weak ferromagnetic coupling. The increase of the SrIrO₃ layer thickness to 12 MLs did not lead to an increase of the coupling but to rather fully decoupled layers. This is most likely related to the electronic properties of the SrIrO₃ spacer, which, unlike LaNiO₃ spacers,¹⁷ does not enable the ferromagnetic coupling of SrRuO₃ layers. The magnetic decoupling of SrRuO₃ by SrIrO₃ spacers is undesirable in the context of skyrmion formation. Without ferromagnetic coupling between the magnetic layers, skyrmions forming in the SrRuO₃ layers cannot be coupled through multilayer stacks. As SrIrO₃ layers turned out to be unsuitable as spacers for

achieving strong magnetic coupling, other oxide layers ought to be considered for realizing this end.

Our study stresses also the scientific relevance of first order reversal curve investigations for the study of magnetic interlayer coupling, being capable to detect even weak coupling interactions as well as to determine whether the coupling is antiferromagnetic or ferromagnetic. Additionally, FORC measurements have the advantage that a correction for the contribution of magnetic impurities is not necessary because the peaks representing the various magnetization reversal steps are well separated in the FORC density maps. We demonstrated that reintegrating the FORC density without the reversible ridge can be an alternative method to correct a sample's hysteresis loop for the cumbersome contributions of soft magnetic impurities, which often affect the magnetometry measurements of thin film samples.

SUPPLEMENTARY MATERIAL

See the [supplementary material](#) for additional information on the sample deposition, the background correction of the SQUID magnetometry data, polar MOKE measurements of heterostructure RIR2, the temperature dependence of the interlayer coupling strength of RIR2, the FORC study of a heterostructure with a 1 ML SrIrO₃/1 ML SrZrO₃ spacer, SQUID magnetometry and magnetotransport study of the heterostructure RIR12, SQUID magnetometry of a second heterostructure with a 2 ML SrIrO₃ spacer, and resistance measurements of heterostructure RIR12, and 6 and 12 ML bare SrIrO₃ reference samples.

ACKNOWLEDGMENTS

We thank René Borowski and Silvia de Waal for etching the STO substrates and Susanne Heijligen for assistance with SQUID measurements. I.L.-V. acknowledges the financial support from the German Research Foundation (DFG) for Project No. 403504808 within SPP2137 and for Project No. 277146847 within SFB1238 (project A01). We are grateful to DFG for the financing of the PLD-RHEED system (Project No. 407456390). L.Y. thanks the China Scholarship Council (File No. 201706750015) for his fellowship.

AUTHOR DECLARATIONS

Conflict of Interest

The authors have no conflicts to disclose.

Author Contributions

L.W. and S.E.I. contributed equally to this work.

DATA AVAILABILITY

The data that support the findings of this study are available from the corresponding author upon reasonable request.

REFERENCES

1. J. Matsuno, N. Ogawa, K. Yasuda, F. Kagawa, W. Koshibae, N. Nagaosa, Y. Tokura, and M. Kawasaki, "Interface-driven topological Hall effect in SrRuO₃-SrIrO₃ bilayer," *Sci. Adv.* **2**, e1600304 (2016).

- ²Y. Ohuchi, J. Matsuno, N. Ogawa, Y. Kozuka, M. Uchida, Y. Tokura, and M. Kawasaki, "Electric-field control of anomalous and topological Hall effects in oxide bilayer thin films," *Nat. Commun.* **9**, 213 (2018).
- ³K.-Y. Meng, A. S. Ahmed, M. Baćani, A.-O. Mandru, X. Zhao, N. Bagnés, B. D. Esser, J. Flores, D. W. McComb, H. J. Hug, and F. Yang, "Observation of nanoscale skyrmions in SrIrO₃/SrRuO₃ bilayers," *Nano Lett.* **19**, 3169–3175 (2019).
- ⁴A. K. Nandy, N. S. Kiselev, and S. Blügel, "Interlayer exchange coupling: A general scheme turning chiral magnets into magnetic multilayers carrying atomic-scale skyrmions," *Phys. Rev. Lett.* **116**, 177202 (2016).
- ⁵C. Moreau-Luchaire, C. Moutafis, N. Reyren, J. Sampaio, C. A. Vaz, N. Van Horne, K. Bouzehouane, K. Garcia, C. Deranlot, P. Warnicke, P. Wohlhüter, J. M. George, M. Weigand, J. Raabe, V. Cros, and A. Fert, "Additive interfacial chiral interaction in multilayers for stabilization of small individual skyrmions at room temperature," *Nat. Nanotechnol.* **11**, 444–448 (2016).
- ⁶S. D. Pollard, J. A. Garlow, J. Yu, Z. Wang, Y. Zhu, and H. Yang, "Observation of stable Néel skyrmions in cobalt/palladium multilayers with Lorentz transmission electron microscopy," *Nat. Commun.* **8**, 14761 (2017).
- ⁷D. J. Groenendijk, C. Autieri, T. C. van Thiel, W. Brzezicki, J. R. Hortensius, D. Afanasiev, N. Gauquelin, P. Barone, K. H. W. van den Bos, S. van Aert, J. Verbeeck, A. Filippetti, S. Picozzi, M. Cuoco, and A. D. Caviglia, "Berry phase engineering at oxide interfaces," *Phys. Rev. Res.* **2**, 023404 (2020).
- ⁸L. Wysocki, J. Schöpf, M. Ziese, L. Yang, A. Kovács, L. Jin, R. B. Versteeg, A. Bliesener, F. Gunkel, L. Kornblum, R. Dittmann, P. H. M. van Loosdrecht, and I. Lindfors-Vrejoiu, "Electronic inhomogeneity influence on the anomalous Hall resistivity loops of SrRuO₃ epitaxially interfaced with 5d perovskites," *ACS Omega* **5**, 5824–5833 (2020).
- ⁹D. Kan and Y. Shimakawa, "Defect-induced anomalous transverse resistivity in an itinerant ferromagnetic oxide," *Phys. Status Solidi B* **255**, 1800175 (2018).
- ¹⁰D. Kan, T. Moriyama, K. Kobayashi, and Y. Shimakawa, "Alternative to the topological interpretation of the transverse resistivity anomalies in SrRuO₃," *Phys. Rev. B* **98**, 180408 (2018).
- ¹¹D. Kan, T. Moriyama, and Y. Shimakawa, "Field-sweep-rate and time dependence of transverse resistivity anomalies in ultrathin SrRuO₃ films," *Phys. Rev. B* **101**, 014448 (2020).
- ¹²Q. Qin, L. Liu, W. Lin, X. Shu, Q. Xie, Z. Lim, C. Li, S. He, G. M. Chow, and J. Chen, "Emergence of topological Hall effect in a SrRuO₃ single layer," *Adv. Mater.* **31**, 1807008 (2019).
- ¹³L. Wu, F. Wen, Y. Fu, J. H. Wilson, X. Liu, Y. Zhang, D. M. Vasiukov, M. S. Kareev, J. H. Pixley, and J. Chakhalian, "Berry phase manipulation in ultrathin SrRuO₃ films," *Phys. Rev. B* **102**, 220406 (2020).
- ¹⁴L. Yang, L. Wysocki, J. Schöpf, L. Jin, A. Kovács, F. Gunkel, R. Dittmann, P. H. M. van Loosdrecht, and I. Lindfors-Vrejoiu, "Origin of the hump anomalies in the Hall resistance loops of ultrathin SrRuO₃/SrIrO₃ multilayers," *Phys. Rev. Mater.* **5**, 014403 (2021).
- ¹⁵L. Wysocki, L. Yang, F. Gunkel, R. Dittmann, P. H. M. van Loosdrecht, and I. Lindfors-Vrejoiu, "Validity of magnetotransport detection of skyrmions in epitaxial SrRuO₃ heterostructures," *Phys. Rev. Mater.* **4**, 054402 (2020).
- ¹⁶S. Esser, J. Wu, S. Esser, R. Gruhl, A. Jesche, V. Roddatis, V. Moshnyaga, R. Pentcheva, and P. Gegenwart, "Angular dependence of Hall effect and magnetoresistance in SrRuO₃-SrIrO₃ heterostructures," *Phys. Rev. B* **103**, 214430 (2021).
- ¹⁷L. Yang, L. Jin, L. Wysocki, J. Schöpf, D. Jansen, B. Das, L. Kornblum, P. H. M. van Loosdrecht, and I. Lindfors-Vrejoiu, "Enhancing the ferromagnetic interlayer coupling between epitaxial SrRuO₃ layers," *Phys. Rev. B* **104**, 064444 (2021).
- ¹⁸G. Herranz, B. Martínez, J. Fontcuberta, F. Sánchez, M. V. García-Cuenca, C. Ferrater, and M. Varela, "SrRuO₃/SrTiO₃/SrRuO₃ heterostructures for magnetic tunnel junctions," *J. Appl. Phys.* **93**, 8035–8037 (2003).
- ¹⁹L. Wysocki, R. Mirzaaghaev, M. Ziese, L. Yang, J. Schöpf, R. B. Versteeg, A. Bliesener, J. Engelmayer, A. Kovács, L. Jin, F. Gunkel, R. Dittmann, P. H. M. van Loosdrecht, and I. Lindfors-Vrejoiu, "Magnetic coupling of ferromagnetic SrRuO₃ epitaxial layers separated by ultrathin non-magnetic SrZrO₃/SrIrO₃," *Appl. Phys. Lett.* **113**, 192402 (2018).
- ²⁰B. Pang, L. Zhang, Y. B. Chen, J. Zhou, S. Yao, S. Zhang, and Y. Chen, "Spin-glass-like behavior and topological Hall effect in SrRuO₃/SrIrO₃ superlattices for oxide spintronics applications," *ACS Appl. Mater. Interfaces* **9**, 3201–3207 (2017).
- ²¹F. Groß, S. E. Ilse, G. Schütz, J. Gräfe, and E. Goering, "Interpreting first-order reversal curves beyond the Preisach model: An experimental permalloy microarray investigation," *Phys. Rev. B* **99**, 064401 (2019).
- ²²F. Bèron, L. Clime, M. Ciureanu, D. Menard, R. Cochrane, and A. Yelon, "First-order reversal curves diagrams of ferromagnetic soft nanowire arrays," *IEEE Trans. Magn.* **42**, 3060–3062 (2006).
- ²³J. Gräfe, M. Weigand, C. Stahl, N. Träger, M. Kopp, G. Schütz, E. J. Goering, F. Haering, P. Ziemann, and U. Wiedwald, "Combined first-order reversal curve and x-ray microscopy investigation of magnetization reversal mechanisms in hexagonal antidot lattices," *Phys. Rev. B* **93**, 014406 (2016).
- ²⁴J. Gräfe, M. Weigand, N. Träger, G. Schütz, E. J. Goering, M. Skripnik, U. Nowak, F. Haering, P. Ziemann, and U. Wiedwald, "Geometric control of the magnetization reversal in antidot lattices with perpendicular magnetic anisotropy," *Phys. Rev. B* **93**, 104421 (2016).
- ²⁵C.-I. Dobrotă and A. Stancu, "What does a first-order reversal curve diagram really mean? A study case: Array of ferromagnetic nanowires," *J. Appl. Phys.* **113**, 043928 (2013).
- ²⁶S. E. Ilse, F. Groß, G. Schütz, J. Gräfe, and E. Goering, "Understanding the interaction of soft and hard magnetic components in NdFeB with first-order reversal curves," *Phys. Rev. B* **103**, 024425 (2021).
- ²⁷S. Muralidhar, J. Gräfe, Y.-C. Chen, M. Etter, G. Gregori, S. Ener, S. Sawatzki, K. Hono, O. Gutfleisch, H. Kronmüller, G. Schütz, and E. J. Goering, "Temperature-dependent first-order reversal curve measurements on unusually hard magnetic low-temperature phase of MnBi," *Phys. Rev. B* **95**, 024413 (2017).
- ²⁸W. Guo, D. X. Ji, Z. B. Gu, J. Zhou, Y. F. Nie, and X. Q. Pan, "Engineering of octahedral rotations and electronic structure in ultrathin SrIrO₃ films," *Phys. Rev. B* **101**, 085101 (2020).
- ²⁹D. J. Groenendijk, C. Autieri, J. Girovsky, M. C. Martínez-Velarte, N. Manca, G. Mattoni, A. M. R. V. L. Monteiro, N. Gauquelin, J. Verbeeck, A. F. Otte, M. Gabay, S. Picozzi, and A. D. Caviglia, "Spin-orbit semimetal SrIrO₃ in the two-dimensional limit," *Phys. Rev. Lett.* **119**, 256403 (2017).
- ³⁰N. Manca, D. J. Groenendijk, I. Pallecchi, C. Autieri, L. M. K. Tang, F. Telesio, G. Mattoni, A. Mccollam, S. Picozzi, and A. D. Caviglia, "Balanced electron-hole transport in spin-orbit semimetal SrIrO₃ heterostructures," *Phys. Rev. B* **97**, 081105 (2018).
- ³¹A. Biswas, K.-S. Kim, and Y. H. Jeong, "Metal insulator transitions in perovskite SrIrO₃ thin films," *J. Appl. Phys.* **116**, 213704 (2014).
- ³²B. Kim, P. Liu, and C. Franchini, "Dimensionality-strain phase diagram of strontium iridates," *Phys. Rev. B* **95**, 115111 (2017).
- ³³J. H. Gruenewald, J. Nichols, J. Terzic, G. Cao, J. W. Brill, and S. S. A. Seo, "Compressive strain-induced metal-insulator transition in orthorhombic SrIrO₃ thin films," *J. Mater. Res.* **29**, 2491–2496 (2014).
- ³⁴J. Xia, W. Siemons, G. Koster, M. R. Beasley, and A. Kapitulnik, "Critical thickness for itinerant ferromagnetism in ultrathin films of SrRuO₃," *Phys. Rev. B* **79**, 140407 (2009).
- ³⁵J. Gräfe, F. Groß, S. E. Ilse, D. B. Boltje, S. Muralidhar, and E. J. Goering, "LeXtender: A software package for advanced MOKE acquisition and analysis," *Meas. Sci. Technol.* **32**, 067002 (2021).
- ³⁶F. Groß, J. C. Martínez-García, S. E. Ilse, G. Schütz, E. Goering, M. Rivas, and J. Gräfe, "GFORC: A graphics processing unit accelerated first-order reversal-curve calculator," *J. Appl. Phys.* **126**, 163901 (2019).
- ³⁷W. Wang, L. Li, J. Liu, B. Chen, Y. Ji, J. Wang, G. Cheng, Y. Lu, G. Rijnders, G. Koster, W. Wu, and Z. Liao, "Magnetic domain engineering in SrRuO₃ thin films," *npj Quantum Mater.* **5**, 73 (2020).
- ³⁸P. A. A. van der Heijden, P. J. H. Bloemen, J. M. Metselaar, R. M. Wolf, J. M. Gaines, J. T. W. M. van Eemeren, P. van der Zaag, and W. J. M. de Jong, "Interlayer coupling between Fe₃O₄ layers separated by an insulating nonmagnetic MgO layer," *Phys. Rev. B* **55**, 11569–11575 (1997).

- ³⁹J. Faure-Vincent, C. Tiusan, C. Bellouard, E. Popova, M. Hehn, F. Montaigne, and A. Schuhl, "Interlayer magnetic coupling interactions of two ferromagnetic layers by spin polarized tunneling," *Phys. Rev. Lett.* **89**, 107206 (2002).
- ⁴⁰M. Matczak, B. Szymański, M. Urbaniak, M. Nowicki, H. Głowiński, P. Kuświk, M. Schmidt, J. Aleksiejew, J. Dubowik, and F. Stobiecki, "Antiferromagnetic magnetostatic coupling in Co/Au/Co films with perpendicular anisotropy," *J. Appl. Phys.* **114**, 093911 (2013).
- ⁴¹J. Gräfe, M. Schmidt, P. Audehm, G. Schütz, and E. Goering, "Application of magneto-optical Kerr effect to first-order reversal curve measurements," *Rev. Sci. Instrum.* **85**, 023901 (2014).
- ⁴²D. B. Fulghum and R. E. Camley, "Magnetic behavior of antiferromagnetically coupled layers connected by ferromagnetic pinholes," *Phys. Rev. B* **52**, 13436–13443 (1995).
- ⁴³J. F. Bobo, H. Kikuchi, O. Redon, E. Snoeck, M. Piecuch, and R. L. White, "Pinholes in antiferromagnetically coupled multilayers: Effects on hysteresis loops and relation to biquadratic exchange," *Phys. Rev. B* **60**, 4131–4141 (1999).
- ⁴⁴L. Néel, "Sur un nouveau mode de couplage entre les aimantations de deux couches minces ferromagnétiques," *C.R. Hebd. Acad. Sci.* **255**, 1676 (1962).
- ⁴⁵J. Moritz, F. Garcia, J. C. Toussaint, B. Dieny, and J. P. Nozières, "Orange peel coupling in multilayers with perpendicular magnetic anisotropy: Application to (Co/Pt)-based exchange-biased spin-valves," *Europhys. Lett.* **65**, 123–129 (2004).
- ⁴⁶J. C. Slonczewski, "Conductance and exchange coupling of two ferromagnets separated by a tunneling barrier," *Phys. Rev. B* **39**, 6995–7002 (1989).
- ⁴⁷P. Bruno, "Theory of interlayer magnetic coupling," *Phys. Rev. B* **52**, 411–439 (1995).
- ⁴⁸B. D. Schrag, A. Anguelouch, S. Ingvarsson, G. Xiao, Y. Lu, P. L. Trouilloud, A. Gupta, R. A. Wanner, W. J. Gallagher, P. M. Rice, and S. S. P. Parkin, "Néel 'orange-peel' coupling in magnetic tunneling junction devices," *Appl. Phys. Lett.* **77**, 2373–2375 (2000).
- ⁴⁹L. E. Nistor, "Magnetic tunnel junctions with perpendicular magnetization: Anisotropy, magnetoresistance, magnetic coupling and spin transfer torque switching," Ph.D. thesis (Universite de Grenoble, 2011).
- ⁵⁰B. Rodmacq, V. Baltz, and B. Dieny, "Macroscopic probing of domain configurations in interacting bilayers with perpendicular magnetic anisotropy," *Phys. Rev. B* **73**, 092405 (2006).
- ⁵¹E. Skoropata, J. Nichols, J. M. Ok, R. V. Chopdekar, E. S. Choi, A. Rastogi, C. Sohn, X. Gao, S. Yoon, T. Farmer, R. D. Desautels, Y. Choi, D. Haskel, J. W. Freeland, S. Okamoto, M. Brahlek, and H. N. Lee, "Interfacial tuning of chiral magnetic interactions for large topological Hall effects in $\text{LaMnO}_3/\text{SrIrO}_3$ heterostructures," *Sci. Adv.* **6**, eaaz3902 (2020).